In-vehicle mm-Wave Channel Model and Measurement

Jiri Blumenstein, Tomas Mikulasek,
Roman Marsalek, Ales Prokes
The Faculty of Electrical Engineering and Communication
Brno University of Technology
Brno, Czech Republic
Email: blumenstein@feec.vutbr.cz

Thomas Zemen
FTW Forschungszentrum
Telekommunikation Wien,
Vienna, Austria

Christoph Mecklenbräuker
Institute of Telecommunications,
Vienna University of Technology,
Vienna, Austria

***Abstract*—This contribution documents and discusses recent wideband radio channel measurements carried out in the intra–vehicle environment. Channels in the millimeter-wave (MMW) frequency band have been measured in 55–65 GHz using open-ended rectangular waveguides.**

We present a channel modeling approach based on a decomposition of spatially specific Channel Impulse Responses (CIRs) into large and small scale fading. The decomposition is done by the Hodrick-Prescott filter. We parametrize the small scale fading utilizing Maximum-likelihood estimates for the parameters of a generalized extreme value (GEV) distribution. The large scale fading is described by a two dimensional polynomial curve. We also compare simulated results with our measurement exploiting the two-sample Kolmogorov-Smirnov test.

I. Introduction

The ever increasing vehicle efficiency goes hand in hand with weight savings. One recognized, yet not fully utilized way to achieve vehicle weight reduction, is to replace relatively heavy and costly cable bundles with wireless links. The current upswing of electrically-propelled vehicles struggling with operating range, stress this issue even further. A modern vehicle contains up to several kilometers of wires weighing easily up to 50 kg [1], while vehicle manufacturers appreciate weight savings in tens of grams. Another significant benefit of wireless communication in the in-vehicle environment is represented by the fact that wireless links are universal, thus the necessity to design model-specific cable bundles is to some extent eliminated. Also, the wireless link installation should be easier.

While providing around 10 GHz of unlicensed bandwidth, MMW short range communication systems could beneficially replace the safety non-critical cable bundles e.g. for rear seat entertainment systems or HD video streaming.

The MMW systems enable the usage of high-gain steerable antennas [2] which seem to be beneficial for in-vehicle communication links. On the other hand, the 60 GHz band suffers from high penetration loss and insignificant diffraction contribution [3].

Authors of [2], [4] dealt with comparing UWB and 60 GHz in-vehicle channels. Their results include the Rician K-factor, RMS delay spread and path-loss but they omit any statistical descriptions. The channel model of in-vehicle ambiance is also not present in the mentioned publications. Moreover, their measurement campaign was performed in slightly different bands (67–70.5 GHz) whereas our measurement was performed in 55–65 GHz.

As discussed in [5], [6], the detailed knowledge of radio channel behavior is of course needed for the physical layer design.

A. Contribution of the paper

- Results of an in-vehicle channel measurement campaign performed in the 55-65 GHz frequency band for different antenna placements and occupancy patterns.
- A channel model describing both large and small scale fading.
- Validation of the simulated Channel Impulse Responses (CIRs) using the two-sample Kolmogorov-Smirnov test [7].

The rest of the paper is organized as follows: Firstly we provide the measurement setup description, then we present our channel modeling approach and its results. The conclusion rounds up the paper.

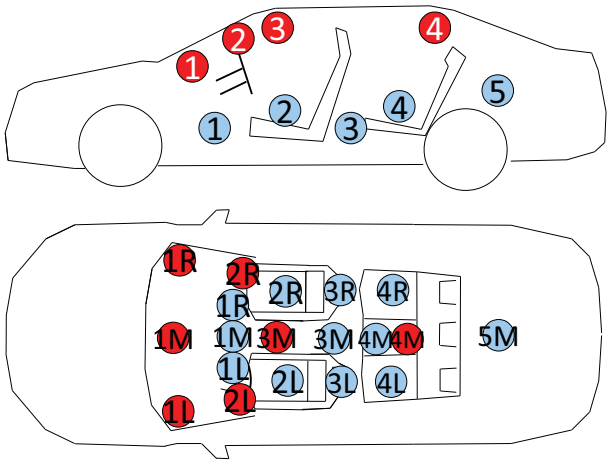

Fig. 1. Antenna placement; RED-receiving antennas, BLUE-transmitting antennas. Measured links between depicted antennas are specified in Table I.

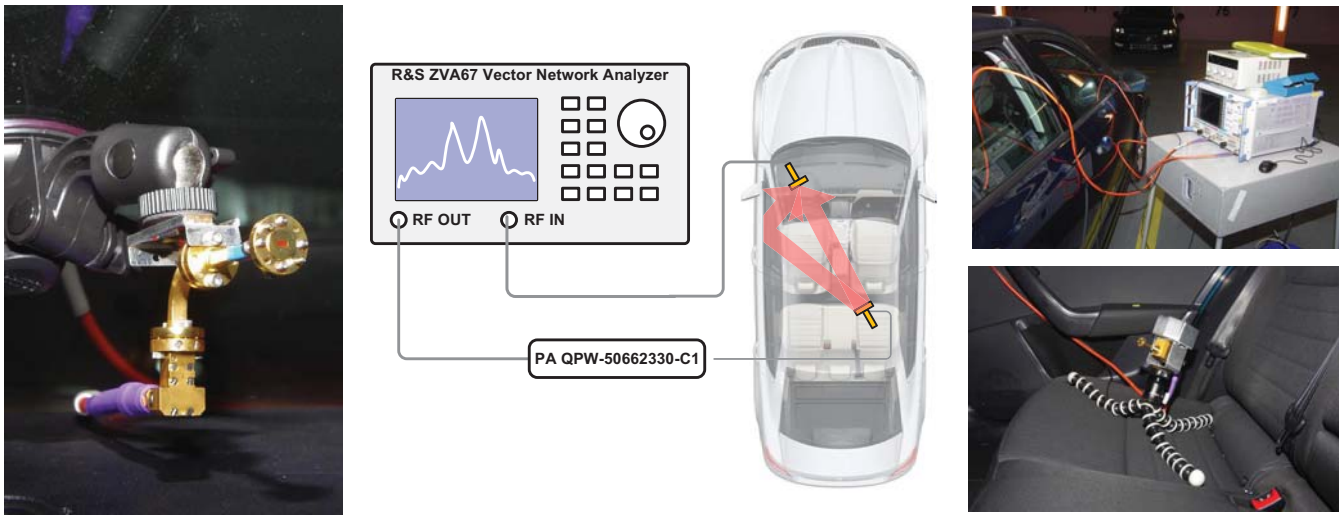

Fig. 2. From left to right: Open waveguide antenna mounted on the front windshield using a suction cup; The diagram of the mm-wave measurement setting with the vector network analyzer, the low noise and power amplifiers type designation; From above: The vector network analyzer next to the measured vehicle; The receiving waveguide antenna mounted on a tripod on the back seat.

II. Measurement Setup

Measurements were performed using the mid-sized passenger car Skoda Octavia III with transmit and receive antennas marked with red and blue colors in Figure 1 respectively. The receiving (RX) antenna was placed at different spatial points inside the car compartment (on all seats, trunk or in front of the seats). The transmitting (TX) antennas were placed on the left and right side of the dash-board and at the rear part of the ceiling according to Figure 1.

The 4-port vector network analyzer R&S ZVA67 (VNA) was used for measuring the transmission coefficient between two antennas in the frequency band 55–65 GHz. The dynamic range of the measurement setup was extended utilizing the broadband power amplifier (QPW-50662330) on the transmitting side. The open waveguide WR15 having the radiation pattern depicted in Figure 3 was used as a transmitting and receiving antenna. The measurement setup was calibrated for zero transmission while the waveguides were connected to each other. The diagram describing the measurement setup for frequency band 55–65 GHz is depicted in Figure 2.

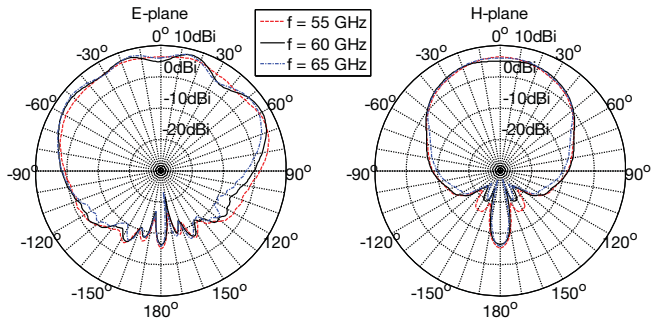

Fig. 3. Simulated gain pattern of the open waveguide in E–plane and H–plane.

TABLE I
Table of antenna positions α with distances between antennas and occupancy.

α	RX ant. pos.	TX ant. pos.	Dist. [cm]	Passangers
1	Outside	4M (Blue)	352	No
2	1R (Red)	4M (Blue)	208	FULL
3	Outside	4M (Blue)	352	No
4	1R (Red)	4M (Blue)	208	D FP RPR RPL
5	1R (Red)	4M (Blue)	208	D
6	1R (Red)	4M (Blue)	208	No
7	1L (Red)	4R (Blue)	170	No
8	4M (Red)	2R (Blue)	165	D
9	2L (Red)	4R (Blue)	148	D
10	1R (Red)	4R (Blue)	149	D
11	2L (Red)	4R (Blue)	148	No
12	1R (Red)	4R (Blue)	149	No
13	1M (Red)	4R (Blue)	162	No
14	1R (Red)	4R (Blue)	149	No
15	1R (Red)	4R (Blue)	149	No
16	1R (Red)	4R (Blue)	149	D
17	1M (Red)	4R (Blue)	162	D
18	4M (Red)	2R (Blue)	165	No
19	4M (Red)	4R (Blue)	88	D
20	1R (Red)	2R (Blue)	72	FP
21	1R (Red)	2R (Blue)	72	No
22	1L (Red)	2R (Blue)	112	FP
23	2R (Red)	4R (Blue)	119	D
24	1L (Red)	2R (Blue)	112	No
25	2R (Red)	4R (Blue)	119	No
26	4M (Red)	4R (Blue)	88	No

Legend: **D**-driver, **FP**-front passenger, **RPR**-rear passenger right, **RPL**-rear passenger left, **FULL**-all passengers, **No**-empty car, **Outside**-outside of the car (not depicted in Figure 1).

III. Channel Description

Since the measurements were performed in the frequency domain with 10 MHz step, we utilized the inverse Fourier transform with a rectangular window to obtain the channel impulse response. Then we employed a peak detector in order

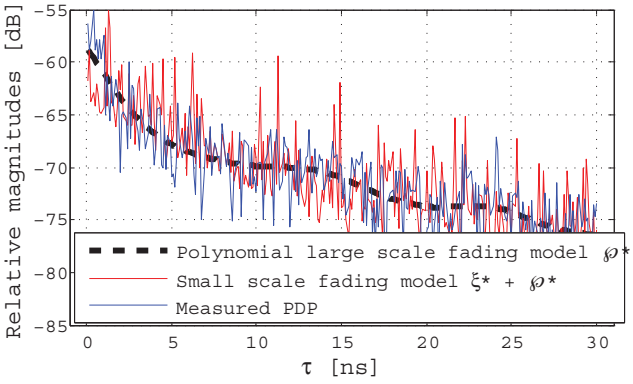

Fig. 4. Comparison of 3-3 order 2D polynomial large scale fading model $\wp^*$, sum of $\wp$ and log-Weibull-distributed small scale fading model ξ^* and measured CIR.

to recognize the first arrival of multipath component of the examined CIR.

A. Channel Impulse Response (CIR)

The intra vehicle environment is considered as time invariant, therefore the multipath wireless channels are described by the impulse response according to:

$$h'_\alpha(\tau) = \sum_{n=0}^{N-1} \rho_n \mathrm{e}^{j\Phi_n} \delta(\tau - \tau_n), \tag{1}$$

where τ_n and $\rho_n \mathrm{e}^{j\Phi_n}$ are the propagation delay and complex gain coefficient of the n-th multipath component. The index α denotes the measurement number according to Table I. The $h_\alpha(\tau)$ is a complex number with phase uniformly distributed in the interval $[0, 2\pi)$. In the following text, we use the absolute value of CIR, $h_\alpha(\tau) =\mid h'_\alpha(\tau) \mid$.

Our hypothesis assumes that CIR is composed of large scale fading and a superimposed small scale fading process. To decompose these components, the exploitation of the Hodrick-Prescott detrending filter [8], which operates with so called cyclical and trend components, is straightforward. When compared with a moving average filter, the Hodrick-Prescott does not cause data loss, thus seems beneficial. In general, however, other approaches are certainly possible.

In the following, we derive the channel model of an in-vehicle environment for 55–65 GHz considering a variety of antenna positions and occupancy configurations (according to Figure 1). This idea is illustrated in Figure 4 taking into account one specific measurement number α. The channel model consists of:

- *large scale fading model* represented by a two dimensional polynomial curve $\wp^*_\alpha(\tau)$ where τ is time in delay domain. Let us note that we use * superscript to mark models of measured variables (written without the * superscript).
- *small scale fading model* represented by the Generalized Extreme Value (GEV) random process $\xi^*(k, \sigma, \mu)$, where k is the shape parameter, σ is the distribution scale parameter and μ is the location parameter [9]. It will be shown, that GEV can be simplified into the log-Weibull-distributed process $\xi^*(0, \sigma, \mu)$.

Therefore we write:

$$h_\alpha(\tau) = \wp_\alpha(\tau) + \xi_\alpha(\tau). \tag{2}$$

B. Large scale fading

First, by filtering the measured $h_\alpha(\tau)$ by the Hodrick-Prescott de-trending filter according to Equation 3, the cyclical component $\xi_\alpha(\tau)$ is obtained.

$$\xi_\alpha(\tau) = \min_{\wp} \left(\sum_{\tau=1}^{T} (h_\alpha(\tau) - \wp_\alpha(\tau))^2 + \right. \tag{3}$$

$$\left. + \lambda \sum_{\tau=2}^{T-1} \left[(\wp_\alpha(\tau+1) - \wp_\alpha(\tau)) - (\wp_\alpha(\tau) - \wp_\alpha(\tau-1)) \right]^2 \right),$$

where $\wp$ represents a trend component and $\tau = 1, \ldots, T$ is the time in delay domain. Let us note that according to the terminology utilized in [8] we consider the cyclical component to represent the small scale variations while large scale fading is described by the trend component.

The heuristically chosen positive multiplier λ adjusts the filter's capability to filter out the short-term fluctuations. This paper utilizes $\lambda = 5e6$, however, the range of exploitable values is from $\lambda = 500$ up to $\lambda = 5e6$, while the lower the λ, the faster the $\wp$ changes. We have chosen the λ in the upper range of usable values in order to provide the polynomial fit of the lowest possible order while still maintaining the two-sample Kolmogorov-Smirnov p-values in the > 0.1 region ensuring a "very significant match" according to the ingrained interpretation of the two-sample Kolmogorov-Smirnov test results. More information regarding the adjustment of the Hodrick-Prescott filter is elaborated in [10].

Next, with accordance to Equation 2, the cyclical component ξ is subtracted from measured $h_\alpha(\tau)$ pursuant to:

$$\wp_\alpha(\tau) = h_\alpha(\tau) - \xi_\alpha(\tau), \tag{4}$$

thus obtaining the large scale fading component $\wp_\alpha(\tau)$. The measured $\wp_\alpha(\tau)$ quantity is visible in Figure 5, where the data is aligned by the first arrival of multipath component detected by the peak detector and sorted according to the mean power such that the large scale fading map is described by the polynomial fit of the lowest possible order.

To model the measured large scale fading phenomena, we parametrize the $\wp_\alpha(\tau)$ utilizing the two dimensional polynomial fit of order 3 in both domains, namely in the delay domain and the spatial domain represented by the variable index α. The 2D polynomial fit is given as:

$$\wp^*_\alpha(\tau) = p_{00} + p_{10}\alpha + p_{01}\tau + p_{20}\alpha^2 + p_{11}\alpha\tau + p_{02}\tau^2 + \tag{5}$$
$$+ p_{30}\alpha^3 + p_{21}\alpha^2\tau + p_{12}\alpha\tau^2 + p_{03}\tau^3,$$

with values of the parameters p_{uw} listed in Table II. The modeled $\wp^*_\alpha(\tau)$ is depicted in Figure 6. Let us note that the measurement index α is treated here as a variable. Otherwise,

if we provided a 1D polynomial fit, we would obtain specific polynomial parameters for each α. Therefore the 2D fit significantly reduces the number of parameters required to describe all measured CIRs.

TABLE II
PARAMETERS OF 3-3 ORDER POLYNOMIAL LARGE SCALE FADING MODEL $\wp^*$

p_{00} = -48.14	p_{02} = 0.0002746
p_{10} = 1.335	p_{30} = 0.0007026
p_{01} = -0.1622	p_{21} = 9.416e-05
p_{20} = -0.05851	p_{12} = -1.254e-05
p_{11} = 0.001221	p_{03} = -4.571e-08

C. Small scale fading

Utilizing the Maximum Likelihood Estimation (MLE), we determined that the best fit for the superimposed small scale fading signal ξ was achieved by using the Generalized Extreme Value (GEV) distribution [9]. The fitted parameters of the signal ξ as well as the measured data are visible in Figure 7. The Probability Density Function (PDF) of the GEV is given by:

$$f(x \mid k, \mu, \sigma) = \frac{1}{\sigma}\exp\left[-\beta^{-\frac{1}{k}}\right]\beta^{-1-\frac{1}{k}}, \tag{6}$$

for

$$\beta = 1 + k\frac{x-\mu}{\sigma}, \tag{7}$$

where μ is the location parameter, k is the shape parameter and σ the distribution scale parameter.

TABLE III
SUMMARIZATION OF GEV PARAMETERS CHARACTERIZING IN-VEHICLE SMALL SCALE FADING IN THE 55-65 GHZ BAND FOR 26 PERMUTATIONS OF ANTENNA PLACEMENT AND CAR SEAT OCCUPANCY.

55-65 GHz	Dist. type	Mean ν	Variance η
shape parameter k	GEV	-0.0902	0.0031
scale parameter σ	GEV	4.81	0.1004
location parameter μ	GEV	-2.317	0.0308

As will be documented by the Kolmogorov-Smirnov test results, the small scale fading model ξ^* can be approximated by the log-Weibull (also called as Gumbel) distribution [11]. For a specific choice of parameters, the log-Weibull reduces to the Weibull distribution. The Weibull distribution of path fading is presented in [12], [13].

In [14] the author claims that there is no theoretical explanation for encountering this distribution type. On the other hand, it contains the well accepted Rayleigh distribution as a special case. The best MLE fit is produced by the log-Weibull distribution probably due to the fact that this distribution exploits three parameters which enhances the flexibility to match the empirical data.

IV. VALIDATION AND UTILIZATION OF THE PRESENTED CHANNEL MODEL

The presented channel model consists of:

- The map of large scale fading $\wp^*_\alpha(\tau)$ presented in Figure 6. This map models the measured large scale fading component $\wp_\alpha(\tau)$ extracted from $h_\alpha(\tau)$ utilizing the Hodrick-Prescott detrending filter. In Figure 5, the order of link index α in $\wp_\alpha(\tau)$ is sorted such that the mean power is increasing with increasing α. Thus, the polynomial fit is of the lowest possible order while still maintaining p-values of the Kolmogorov-Smirnov test higher than 0.1.
- The log-Weibull-distributed random process ξ^* with parameters according to Table III which is superimposed to the large scale fading $\wp^*_\alpha(\tau)$.

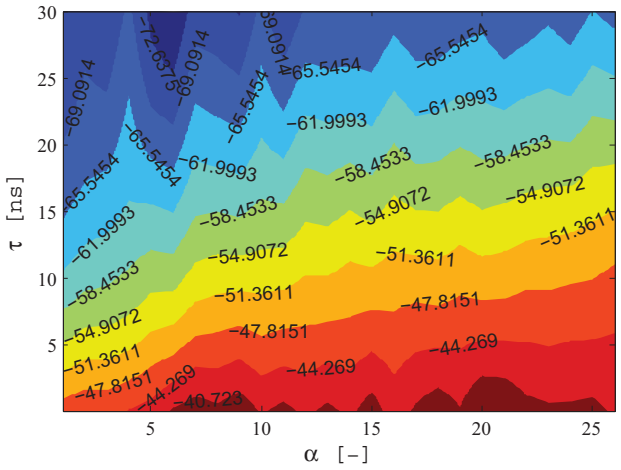

Fig. 5. Measured large scale fading component $\wp_\alpha(\tau)$ representing $h_\alpha(\tau)$ filtered by the Hodrick-Prescott filter using λ=5e6. The data is aligned by the first arrival of multipath component detected by a peak detector and sorted according to the mean power, thus the large scale fading map is described by the polynomial fit $\wp^*$ of the lowest possible order. The values α denotes spatially specific wireless link indexes according to Table I and Figure 1. Values attached to the contours are in dB.

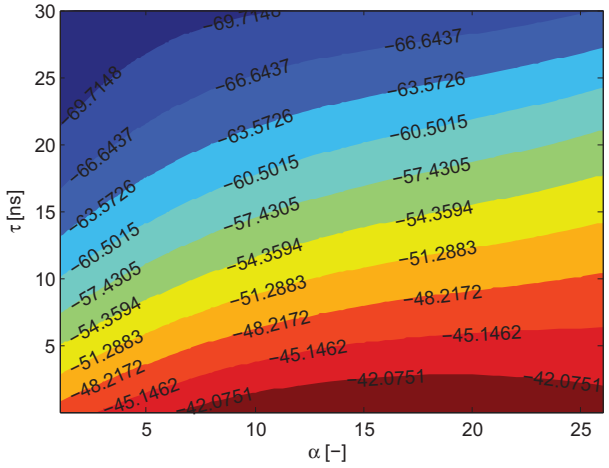

Fig. 6. Large scale fading map $\wp^*_\alpha(\tau)$ representing the polynomial 3-3 order model of $h_\alpha(\tau)$ filtered by the Hodrick-Prescott filter. Values attached to the contours are in dB.

A. Utilization of the channel model

Let us assume, that we are concerned about recreating the CIR for the wireless link between the RX 4M and TX 2R

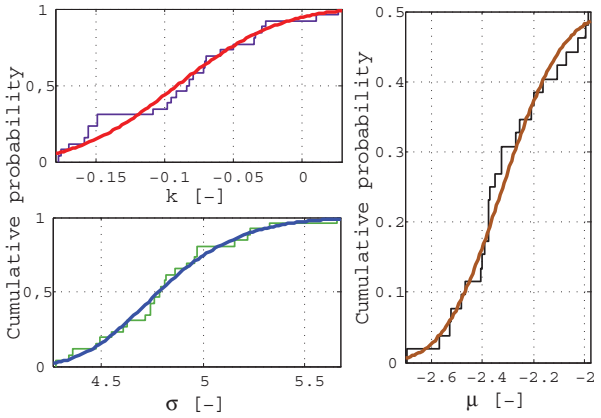

Fig. 7. Cumulative probability of ξ representing small scale fading superimposed to $\wp^*$ model. The small scale fading signal ξ is fitted with Generalized extreme value distribution according to Table III which can be further simplified to the log-Weibull-distributed signal ($k = 0$).

antennas according to Figure 1. The maximal delay spread is for example $\tau_{\max}$ =30 ns. Our maximal time resolution T_{r} is given by the 10 GHz bandwidth as $T_{\mathrm{r}} = 1/10e9$. From Table 1 it is seen, that this configuration is marked as $\alpha = 8$. Next, $\alpha = 8$ is substituted to Equation 5, while τ linearly increases from T_{r} up to the product of $\tau_{\max}$ and T_{r}. The result of Equation 5 is the large scale fading model $\wp_8^*$. The small scale fading ξ^* is obtained using the GEV generator with settings according to Table III. The modeled CIR is then written as: $h'_8(\tau) = [\wp_8^*(\tau) + \xi_8^*(\tau)]e^{j\phi}$, where the phase ϕ is uniformly distributed in the interval $[0, 2\pi)$.

B. Validation of the channel model

In order to validate our in-vehicle channel model, in Figure 8 we provide results of the two-sample Kolmogorov-Smirnov test representing a commonly used metric for goodness of fit. Figure 8 shows the resulting p-values where only two cases fall into sub 0.1 region, however, all other cases are in the > 0.1 area.

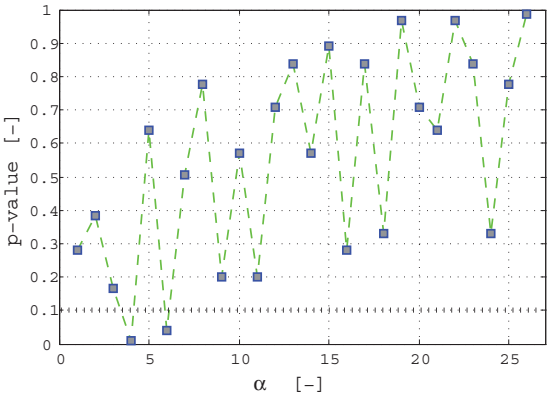

Fig. 8. p-value of the Kolmogorov-Smirnov test comparing measured CIR and polynomial CIR model $\wp^*$ of large scale fading with input parameters according to Table II with superimposed log-Weibull-distributed small scale fading model $\xi^*(0, 4.394, -2)$.

V. Conclusion

This paper deals with the in-vehicle channel measurement campaign carried out in the 55-65 GHz band and provides a corresponding channel model including a simple application example. The channel model operates with the fundamental hypothesis of decomposition of the CIR into large scale and small scale fading. The decomposition is performed using the Hodrick-Prescott filter. The large scale fading is then simulated with a two-dimensional polynomial curve while the small scale fading is modeled with the log-Weibull-distributed random process. Finally, we present the resulting p-values of the two-sample Kolmogorov-Smirnov test showing no disagreement with our hypothesis.

Acknowledgment

This work was supported by the Czech Science Foundation project No. 13- 38735S Research into wireless channels for intra-vehicle communication and positioning, and was performed in laboratories supported by the SIX project, No. CZ.1.05/2.1.00/03.0072, the operational program Research and Development for Innovation. The cooperation in the COST IC1004 action was supported by the MEYS of the Czech Republic project no. LD12006 (CEEC). The Skoda a.s. Mlada Boleslav and Christian Doppler Laboratory for Wireless Technologies for Sustainable Mobility are also gratefully acknowledged.

References

[1] G. Leen and D. Heffernan, "Expanding automotive electronic systems," *Computer*, vol. 35, no. 1, pp. 88–93, 2002.

[2] E. Ben-Dor, T. Rappaport, Y. Qiao, and S. Lauffenburger, "Millimeter-wave 60 GHz outdoor and vehicle AOA propagation measurements using a broadband channel sounder," in *Global Telecommunications Conference (GLOBECOM 2011), 2011 IEEE*, Dec 2011, pp. 1–6.

[3] C. Gustafson, K. Haneda, S. Wyne, and F. Tufvesson, "On mm-wave multi-path clustering and channel modeling," 2014.

[4] M. Schack, M. Jacob, and T. Kurner, "Comparison of in-car UWB and 60 GHz channel measurements," in *Antennas and Propagation (EuCAP), 2010 Proceedings of the Fourth European Conference on*. IEEE, 2010, pp. 1–5.

[5] S. Krone, F. Guderian, G. Fettweis, M. Petri, M. Piz, M. Marinkovic, M. Peter, R. Felbecker, and W. Keusgen, "Physical layer design, link budget analysis, and digital baseband implementation for 60 GHz short-range applications," *International Journal of Microwave and Wireless Technologies*, vol. 3, no. 02, pp. 189–200, 2011.

[6] J. Blumenstein, R. Marsalek, A. Prokes, and C. Mecklenbrauker, "Impulse noise mitigation for OFDM by time-frequency spreading," in *Multiple Access Communcations*, 2013.

[7] F. J. Massey Jr, "The Kolmogorov-Smirnov test for goodness of fit," *Journal of the American statistical Association*, vol. 46, no. 253, pp. 68–78, 1951.

[8] R. J. Hodrick and E. C. Prescott, "Postwar US business cycles: an empirical investigation," *Journal of Money, credit, and Banking*, pp. 1–16, 1997.

[9] S. Kotz and S. Nadarajah, *Extreme value distributions*. World Scientific, 2000.

[10] M. O. Ravn and H. Uhlig, "On adjusting the Hodrick-Prescott filter for the frequency of observations," *Review of economics and statistics*, vol. 84, no. 2, pp. 371–376, 2002.

[11] E. Gumbel, "Les valeurs extrêmes des distributions statistiques," in *Annales de l'institut Henri Poincaré*, vol. 5, no. 2. Presses universitaires de France, 1935, pp. 115–158.

[12] N. Shepherd, "Radio wave loss deviation and shadow loss at 900 MHz," *Vehicular Technology, IEEE Transactions on*, vol. 26, no. 4, pp. 309–313, Nov 1977.

[13] S. Howard and K. Pahlavan, "Fading results from narrowband measurements of the indoor radio channel," in *Personal, Indoor and Mobile Radio Communications., IEEE International Symposium on*, Sep 1991, pp. 92–97.

[14] H. Hashemi, "The indoor radio propagation channel," *Proceedings of the IEEE*, vol. 81, no. 7, pp. 943–968, 1993.